Journal of Molecular Graphics and Modelling 59 (2015) 100–106

Contents lists available at ScienceDirect

Journal of Molecular Graphics and Modelling

journal homepage: www.elsevier.com/locate/JMGM

Theoretical investigation of self-assembled donor–acceptor phthalocyanine complexes and their application in dye-sensitized solar cells

Lijuan Yu[a,b], Li Lin[b], Yuwen Liu[b], Renjie Li[b,*]

[a] Yangtze River Fisheries Research Institute, Chinese Academy of Fishery Sciences, Wuhan 430223, PR China
[b] College of Chemistry and Molecular Science, Wuhan University, Wuhan 430072, PR China

ARTICLE INFO

Article history:
Accepted 3 April 2015
Available online 13 April 2015

Keywords:
Zinc phthalocyanine
Density functional calculations
Dye-sensitized solar cell
Self-assembled
Axial coordination

ABSTRACT

A theoretical investigation of self-assembled donor–acceptor dyads (**ZnPca**, **ZnPcb** and **ZnPcc**) formed by axial coordination of zinc phthalocyanines appended with 4-carboxyl pyridine has been conducted with the density functional theory (DFT) method and time-dependent DFT (TD-DFT) calculations. A comparison between the molecular structures, atomic charges, molecular orbitals, UV–vis spectra and infrared (IR) spectra has been studied. Further, as sensitizers for the TiO_2-based dye-sensitized solar cells, the photovoltaic performances have been investigated. The **ZnPcc**-sensitized solar cell exhibits a higher conversion efficiency than the **ZnPcb** and **ZnPca**-sensitized ones under AM 1.5 G solar irradiation, while the **ZnPca**-sensitized cell performs the poorest due to the lack of peripheral substituents (*n*-butyoxyl groups) which can be confirmed by the result of the theoretical research. It shows that the directionality of charge transfer in the self-assembled donor–acceptor dyads is important and benefit for the efficiency of the DSSC.

1. Introduction

Studies on donor–acceptor dyads capable of undergoing light-induced electron or energy transfer are of current interest to mimic the primary events of the photosynthetic reaction center and also to develop molecular electronic devices [1–8]. Moreover, a large number of innovative researches are emerging, and remarkable achievements have been obtained. Toward constructing such dyads, porphyrins and phthalocyanines have been widely used as a energy/electron donor/acceptor due to their close resemblance to the photosynthetic pigment, chlorophyll, and the established synthetic methodologies [9,10]. Benzoquinone, methyl viologen, fullerene and perylene imides are particularly appealing as electron acceptors [11–15]. Self-assembly via metal–ligand axial coordination is one of the successful approaches developed to study photoinduced electron transfer in donor–acceptor dyads [16–19]. Spectroscopic, redox, and photochemical behavior of self-assembled donor–acceptor dyads formed by axial coordination of tetraphenylporphyrins and fulleropyrrolidine bearing either pyridine or imidazole coordinating ligands were investigated [20,21]. Majima and coworkers reported that the charge transfer of porphyrins and phthalocyanines to the axial ligand, pyromellitic imide, which acts as acceptors [22]. Singlet-singlet energy transfer in self-assembled via axial coordination of imidazole-appended free-base tetraphenylporphyrin, H_2PIm, to either zinc phthalocyanine, ZnPc, or zinc naphthalocyanine, ZnNc, dyads was investigated in noncoordinating solvents [23]. Although there are a lot of reports on the charge transfer of self-assembled donor–acceptor dyads, there are few reports about the appliaction of the dyads in dye-sensitized solar cells (DSSCs).

Phthalocyanines are well known chromophores for their intense absorption in the UV/blue (Soret band) and the red/near IR (Q band) spectral regions, as well as for their excellent electrochemical, photochemical and thermal stability. Furthermore, proper choice of substituents at the periphery of the macrocycle or metal coordination not only can adjust the photoelectrochemical properties, but also can effectively inhibit the aggregation and improve the solubility of phthalocyanines. In the above self-assembled donor–acceptor dyads, zinc porphyrins/phthalocyanines exist as electron donors with axial ligand containing carboxyl groups, phosphonic acid groups or sulfonic acid groups which can be coupled with TiO_2 semiconductor as electron acceptors. Electrons transfer from zinc porphyrin/phthalocyanine to the electron acceptor, and then inject into TiO_2 conduction band from the carboxyl group, phosphonic

* Corresponding author. Tel.: +86 27 6875 2237; fax: +86 27 6875 2237.
E-mail address: lirj@whu.edu.cn (R. Li).

http://dx.doi.org/10.1016/j.jmgm.2015.04.005
1093-3263/

acid group or sulfonic acid group in the electron acceptor. It is possible to achieve directional charge transfer to the conduction band of TiO_2 semiconductor. Therefore, it is probable to realize the application of the dyads in DSSC.

In the present study, self-assembled donor–acceptor phthalocyanine complexes **ZnPca**, **ZnPcb** and **ZnPcc** were formed by axial coordination of symmetrical ZnPc, β-ZnPc(OBu)$_4$ and α-ZnPc(OBu)$_4$ appended with 4-carboxyl pyridine, respectively, and a theoretical study for the molecular structures, atomic charges, molecular orbital energy gaps, molecular orbital spatial distribution, UV–vis absorption spectra, as well as infrared (IR) spectra of the self-assembled donor–acceptor dyads based on density functional theory was conducted. In addition to the theoretical investigations, to further confirm the directional charge transfer in the dyads, **ZnPca**, **ZnPcb** and **ZnPcc** have been used as dye sensitizers to sensitize TiO_2, and their performances in DSSC have been explored. Both experimental and theoretical studies have demonstrated the directional charge transfer in the dyads.

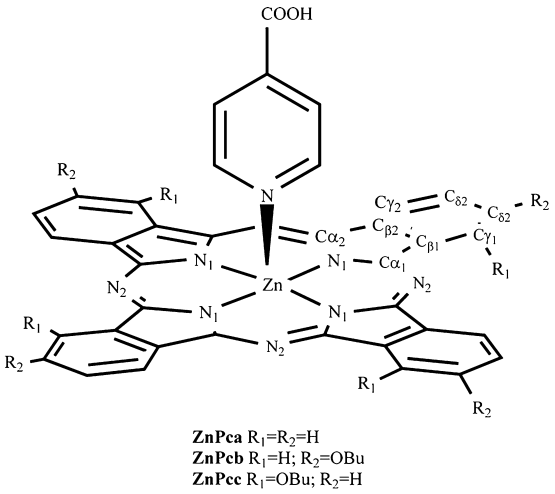

Fig. 1. Molecular structure and atom labeling of **ZnPca**, **ZnPcb** and **ZnPcc**.

2. Experiments

2.1. Chemicals and Instrumentation

Zinc phthalocyanine (ZnPc), 1,8,15,22-tetrakis (*n*-butyoxyl) zinc phthalocyanine (α-ZnPc(OBu)$_4$) and 2,9,16,23-tetrakis (*n*-butyoxyl) zinc phthalocyanine (β-ZnPc(OBu)$_4$) were synthesized according to reported procedures [24,25]. All of the other reagents and solvents were used as received. The dye-sensitized solar cells were fabricated and tested according to our previous study [26,27].

2.2. Computational details

In this paper, the density functional B3LYP (Becke–Lee–Young–Parr composite of exchange–correlation functional) method was used to calculate the structures and vibration properties with LANL2DZ basis set [28–31]. In all work, the LANL2DZ basis set was used for the central metal atoms, and the 6-31G(d) basis set was used for the other atoms. Charge distribution was carried out using a full natural bond orbital analysis (NBO) population method based on the minimized structure with NBO 3.1 in the Gaussian 03 program. The UV–vis absorption spectra were calculated using the TD-DFT method based on the optimized structures with forty singlet-excited states. Gaussian bands with half-bandwidths of 500 cm^{-1} were used to simulate the UV–vis absorption spectra. For all case, B3LYP method and LANL2DZ basis set were used. All calculations were carried out using the Gaussian 03 program in the IBM P690 system in Shandong Province High Performance Computing Centre.

3. Results and discussion

3.1. Molecular structures

The primal input structure of **ZnPca** was obtained by putting Zn^{2+} ions into the central cavity of the phthalocyanine dianion, and one 4-carboxyl pyridine molecule was further introduced at the axial position of ZnPc; *n*-butyoxyl groups were added at the non-peripheral β position of the optimized structure of ZnPc to construct molecule **ZnPcb**; *n*-butyoxyl groups were added at the non-peripheral α position of the optimized structure of ZnPc to construct molecule **ZnPcc**.

The structure and atom labeling of **ZnPca**, **ZnPcb** and **ZnPcc** are shown in Fig. 1, and the main structural parameters of **ZnPca**–**ZnPcc** taken from the calculation results are listed in Table 1. No imaginary vibration was found in the following frequency calculations of the three complexes, indicating that the energy minimized structures of the three complexes are at the true energy minimum.

Analysis of the calculated structural parameters for **ZnPca**, **ZnPcb** and **ZnPcc** shows that the sizes of the central hole (N—N distance) are 4.124, 4.120 and 4.124 Å, respectively. That's to say, peripheral substituents have little effect on the sizes of the central hole. The electron-donating groups at the peripheral positions does not change the circle radius formed by the four isoindole N atoms, which in complete accord with the previous research results [32]. According to our calculations, no significant change of bond length and bond angle is induced by *n*-butyoxyl groups substituted at the peripheral positions of the phthalocyanine complexes. However, the central metal Zn is further pulled out of the molecular plane by the strong attraction of the nitrogen atom according to the calculation results. At the same time, the isoindole N atoms are drawn off the primary plane of the Pc ring due to the restriction of the Zn—N bond length. It is also true for the other atoms on the phthalocyanine macrocycle. Moreover, the relative angle of 4-carboxyl pyridine relative to isoindole unit is 89.9°. Consequently, the molecular symmetry is decreased to C_1 for **ZnPca**, **ZnPcb** and **ZnPcc**.

Table 1
The main structural parameters (bond length/Å and bond angle/°) of **ZnPca**, **ZnPcb** and **ZnPcc** taken from the calculation results.

Parameters	ZnPca	ZnPcb	ZnPcc
Zn—N_1	2.062	2.060	2.062
N_1—$C_{\alpha1}$	1.389	1.388	1.386
N_1—$C_{\alpha2}$	1.389	1.391	1.394
$C_{\alpha1}$—$C_{\beta1}$	1.471	1.472	1.470
$C_{\beta1}$—$C_{\gamma1}$	1.403	1.403	1.403
$C_{\beta2}$—$C_{\gamma2}$	1.403	1.407	1.415
$C_{\gamma1}$—$C_{\delta1}$	1.408	1.410	1.404
$C_{\gamma2}$—$C_{\delta2}$	1.408	1.400	1.415
$C_{\delta1}$—$C_{\delta2}$	1.419	1.423	1.415
N_1—Zn—N_1	88.28	88.38	88.29
Zn—N_1—$C_{\alpha1}$	125.37	125.45	124.52
N_1—$C_{\alpha1}$—N_2	127.04	127.11	127.15
N_1—$C_{\alpha1}$—$C_{\beta1}$	108.60	108.59	108.54
$C_{\alpha2}$—N_2—$C_{\alpha1}$	125.58	125.66	125.80
N_2—$C_{\alpha1}$—$C_{\beta1}$	124.34	124.29	123.30
$C_{\alpha1}$—$C_{\beta1}$—$C_{\beta2}$	106.66	106.61	106.94
$C_{\alpha1}$—$C_{\beta1}$—$C_{\gamma1}$	132.24	131.49	130.42
$C_{\beta1}$—$C_{\beta2}$—$C_{\gamma2}$	121.10	120.42	119.55
$C_{\beta1}$—$C_{\gamma1}$—$C_{\delta1}$	117.83	117.18	117.18
$C_{\gamma1}$—$C_{\delta1}$—$C_{\delta2}$	121.08	121.26	121.42

Table 2
Atomic charges (in *e*) for **ZnPca**, **ZnPcb** and **ZnPcc**.

Atomic charge	ZnPca	ZnPcb	ZnPcc
Zn	1.702	1.697	1.694
N_1	−0.767	−0.772	−0.778
N_2	−0.522	−0.524	−0.523
$C_{\alpha1}$	0.437	0.437	0.435
$C_{\alpha2}$	0.446	0.446	0.440
$C_{\beta1}$	−0.078	−0.057	−0.060
$C_{\beta2}$	−0.077	−0.093	−0.119
$C_{\gamma1}$	−0.186	−0.282	−0.203
$C_{\gamma2}$	−0.185	−0.179	−0.211
$C_{\delta1}$	−0.211	−0.330	−0.303
$C_{\delta2}$	−0.211	−0.241	−0.303
$H_{\alpha1}$	0.237	0.239	0.241
$H_{\alpha2}$	0.237	0.240	
$H_{\beta1}$	0.225		0.223
$H_{\beta2}$	0.225	0.238	0.224

3.2. Atomic charges

Table 2 lists the atomic charges (in *e*) of the skeleton atoms calculated with NBO population method. As shown in Figs. S1–S3 and Tables S1–S3 in the supporting information, the charge distribution on all atoms for **ZnPca**, **ZnPcb** and **ZnPcc** has been given. Substitution of *n*-butyoxyl groups on the peripheral benzene ring of the phthalocyanine structure makes the charges of the Zn, N_1, and N_2 atoms more negative, whereas the charges of the $H_{\alpha1}$ atoms become more positive. The charge of Zn decreases from **ZnPca** (1.702*e*) to **ZnPcc** (1.694*e*), which suggests the stronger metal–ligand reciprocity caused by *n*-butyoxyl groups, so the atomic charge of Zn atom in **ZnPca** is most positive. As a result, the introduction of the electron-donating groups greatly influences the charge distribution on **ZnPcb** and **ZnPcc**, especially on the central metals. What's more, the carbon atoms except $C_{\beta1}$ and $C_{\gamma2}$ have negative charge and their charge decreases from **ZnPca** to **ZnPcc**. It can be seen from Table 2 that the differences in the charge of $C_{\gamma1}$, $C_{\gamma2}$, $C_{\delta1}$ and $C_{\delta2}$ atoms are larger compared with the other carbon atoms for **ZnPca**, **ZnPcb** and **ZnPcc**. This indicates that the substituents of the electron-withdrawing groups have more influence to the charges of $C_{\gamma1}$, $C_{\gamma2}$, $C_{\delta1}$ and $C_{\delta2}$ atoms [32]. As shown in Figs. S1–S3 and Tables S1–S3 in the supporting information, the total charge distribution on axial ligand **ZnPca**, **ZnPcb** and **ZnPcc** is only 0.036*e*, 0.036*e* and 0.035*e*, respectively. So charge transfer in the self-assembled donor–acceptor dyads should be photogeneration, not doping induced.

3.3. Molecular orbital energies

Fig. 2 shows the energy levels of frontier molecular orbitals and energy gaps between the highest occupied molecular orbitals (HOMO) and the lowest unoccupied molecular orbitals (LUMO) of **ZnPca**, **ZnPcb** and **ZnPcc** complexes and Table 3 summarizes

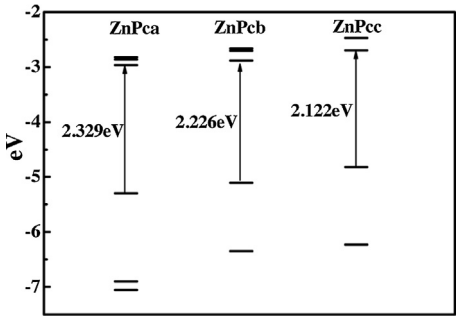

Fig. 2. Orbital energies of **ZnPca**, **ZnPcb** and **ZnPcc**.

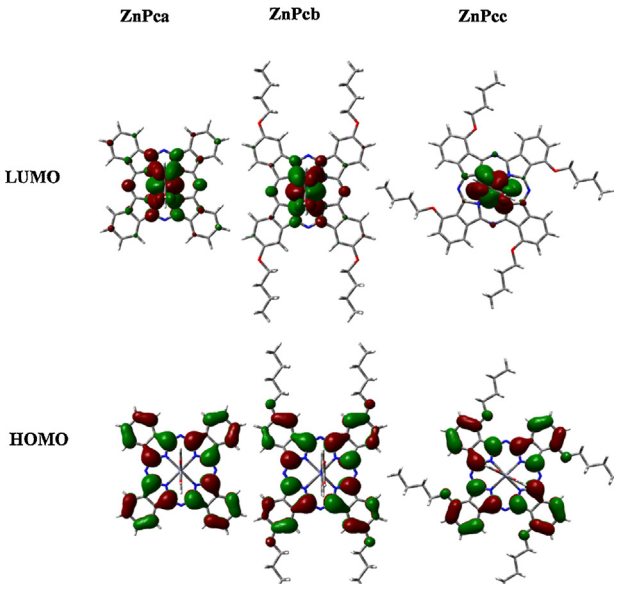

Fig. 3. Molecular orbital distributions of **ZnPca**, **ZnPcb** and **ZnPcc**.

the corresponding energy data. As can be seen, the energy gaps of **ZnPca**, **ZnPcb** and **ZnPcc** gradually decrease along with the moving up of the whole energy levels. According to the gaps, it can be expected that the Q bands of the UV–vis absorption spectra should shift to the longer wavelength side in the same order. Compared with that of **ZnPca**, the narrower bandgaps of **ZnPcb** and **ZnPcc** complexes are due to the introduction of *n*-butyoxyl groups which extend the electron delocalization over the whole molecules. The LUMO levels of **ZnPca**, **ZnPcb** and **ZnPcc** complexes are −2.966 eV, −2.881 eV and −2.697 eV, while the HOMO energy levels are −5.295 eV, −5.107 eV and −4.889 eV, respectively. That's to say, *n*-butyoxyl groups at α positions for **ZnPcc** have a greater impact on the levels than that at β positions for **ZnPcb**. As a result, the LUMO energy levels are more positive than the TiO_2 conduction band (−3.9 eV), and the HOMO energy levels are more negative than the I_3^-/I^- redox potential (−4.9 eV) [33]. Therefore, in DSSC, there is theoretically enough driving force for the regeneration of the excited complexes through recapturing electrons from I^- in the electrolyte. Moreover, the excited state of the electrons have sufficient driving force to inject into the conduction band of TiO_2. In addition, the LUMO levels of **ZnPcb** and **ZnPcc** shift toward higher binding energys, resulting in larger differences between LUMO levels and TiO_2 conduction band. Namely, the driving force for the excited electrons of **ZnPcb** and **ZnPcc** injecting into the TiO_2 conduction band become lager, which may gradually cause the improvement of the DSSC performances. It can also be inferred that the photovoltaic performance of **ZnPcc** may be better than that of **ZnPcb**.

3.4. The molecular orbital spatial distribution

To gain an insight into the molecular orbital spatial distributions of **ZnPca**, **ZnPcb** and **ZnPcc** complexes as well as the charge transport, density functional theory (DFT) calculation was carried out within the framework of the DFT method at the B3LYP/6-31G(d) level. The molecular orbital spatial distributions of HOMOs and LUMOs of the series of self-assembled complexes are very similar, indicating that the introduction of *n*-butyoxyl groups does not change the inherent orbital characters. As observed in Fig. 3, the HOMOs of **ZnPca**, **ZnPcb** and **ZnPcc** complexes are mainly localized at the central phthalocyanine rings, while the LUMOs are much more aligned with 4-carboxyl pyridine at the axial positions,

Table 3
Calculated energy data (in eV) of the frontier molecular orbitals of **ZnPca**, **ZnPcb** and **ZnPcc**.

Molecules	HOMO − 2	HOMO − 1	HOMO	LUMO	LUMO + 1	LUMO + 2
ZnPca	−7.054	−6.898	−5.295	−2.966	−2.864	−2.823
ZnPcb	−6.349	−6.347	−5.107	−2.881	−2.704	−2.663
ZnPcc	−6.234	−6.227	−4.819	−2.697	−2.475	−2.468

which indicates good electron-separated states. The photoexcited electrons would transfer from the phthalocyanine skeleton to the carboxyl group in 4-carboxyl pyridine during the excitation process, which is a benefit to the injection of the photoexcited electrons to the conduction band of the semiconductor [34]. Thus, the directionality of charge transfer in the self-assembled donor–acceptor dyads is theoretically possible.

3.5. UV–vis absorption spectra

The simulated UV–vis absorption spectra of self-assembled donor–acceptor dyads **ZnPca**, **ZnPcb** and **ZnPcc** are shown in Fig. 4. The UV–vis absorption spectra of substituted **ZnPcb** and **ZnPcc** complexes have many differences from that of **ZnPca**, indicating that the peripheral substituents affect the π molecular orbitals of the ring to differing extents. The two curves of **ZnPcb** and **ZnPcc**, as shown in the figure, have very similar shapes and have identical numbers of absorption bands. The only difference is the position of all of the absorption bands of the **ZnPcc** red shift compared with **ZnPcb**. The absorption spectra for **ZnPca**, **ZnPcb** and **ZnPcc** consist of Soret bands at 328, 340 and 365 nm and Q-bands at 583, 591 and 612 nm, respectively. As can be seen, the absorption bands of **ZnPcc** are mostly red-shifted among these compounds, which corresponds well with its smallest HOMO–LUMO gap. And the Q-band of **ZnPca** appears at the shorter wavelength side than those of **ZnPcb** and **ZnPcc** due to the larger energy gap. The red shifts of the absorption spectra for **ZnPcb** and **ZnPcc** can be attributed to the substituted *n*-butyoxyl groups extend the electron delocalization over the whole phthalocyanine molecules [35]. As described in molecular orbital energies, the bandgap of **ZnPcc** with *n*-butyoxyl groups introduced at α positions of phalocyanine ring is narrower than that of **ZnPcb** substituted at β positions. Therefore, the red shifts of the absorption spectra for **ZnPcc** are larger compared to **ZnPcb**.

Furthermore, Table 4 organizes the main peaks, their corresponding oscillator strength, and the nature of the electronic transitions. The calculation results reveal that the Q band is mainly due to the electron transition from HOMO to LUMO + 1 or LUMO + 2, and thus, should correspond with the energy gap of HOMO–LUMO. According to the calculation, Soret bands and Q-bands include the absorption bands corresponding to the charge transition from phthalocyanine to 4-carboxyl pyridine for **ZnPca**, **ZnPcb** and **ZnPcc**, respectively.

Table 4
Calculated wavelength (λ/nm), oscillator strength (*f*), and electron transition nature in the electronic absorption spectra of **ZnPca**, **ZnPcb** and **ZnPcc**.

	λ (nm)	*f*	Electronic transition nature [H = HOMO, L = LUMO]
ZnPca	330.20	0.4882	H-6- > L + 0(58%)
	326.79	0.6887	H-6- > L + 1(56%)
	538.66	0.4011	H-0- > L + 1(61%)
	582.00	0.3707	H-0- > L + 2(58%)
ZnPcb	340.96	0.9571	H-5- > L + 2(52%)
	338.04	0.6886	H-5- > L + 1(55%)
	602.46	0.3978	H-0- > L + 1(60%)
	584.36	0.4243	H-0- > L + 2(61%)
ZnPcc	365.82	0.2632	H-4- > L + 2(43%)
	363.87	0.2598	H-4- > L + 1(51%)
	614.56	0.4346	H-0- > L + 1(42%)
	610.96	0.4536	H-0- > L + 1(52%)

3.6. Infrared spectra

The calculated infrared spectra of **ZnPca**, **ZnPcb** and **ZnPcc** are shown in Fig. 5. As can be seen from Fig. 5, the IR spectra of *n*-butyoxyl groups substituted **ZnPcb** and **ZnPcc** complexes are similar in most peaks, but a few peaks of **ZnPca** have significant differences. The differences can be attributed to the introduction of four *n*-butyoxyl substituents in **ZnPcb** or **ZnPcc**.

Only one relatively weak peak at 3114 cm^{-1} is observed in the simulated spectrum of **ZnPca**, which can be attributed to stretching vibrations of —COOH. However, a couple of new peaks appear in the region of 3066–2800 cm^{-1} for compounds **ZnPcb** and **ZnPcc**, which are clearly due to the symmetrical and asymmetrical C—H stretching modes of the *n*-butyoxyl groups [36]. The vibration peaks below 1700 cm^{-1} for these complexes are quite complicated and actually the mixture of many interrelated vibrational modes. The strongest peak for **ZnPcc** locates at 1201 cm^{-1} is caused by the $C_{\delta 2}$—O unsymmetrical stretching mixed with vibration of phthalocyanine skeleton, which blueshifts to 1211 cm^{-1} for **ZnPcb** due to the fact that the $C_{\gamma 1}$ atoms connected to the O atoms in **ZnPcb** experience a larger steric hindrance than $C_{\delta 2}$ atoms. The fact that

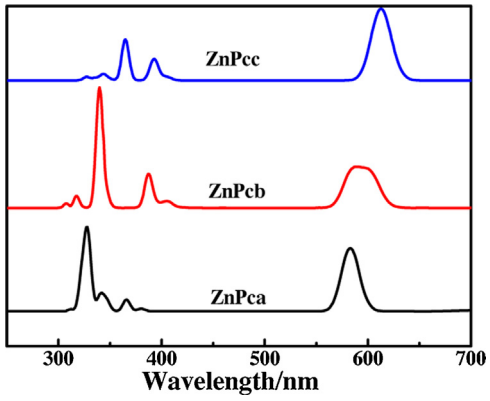

Fig. 4. The simulated UV–vis absorption spectra of **ZnPca**, **ZnPcb** and **ZnPcc**.

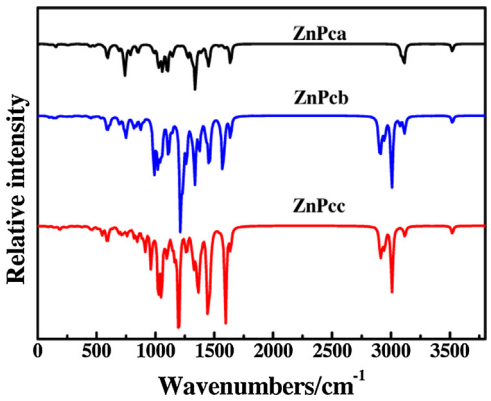

Fig. 5. Simulated IR spectra of **ZnPca**, **ZnPcb** and **ZnPcc**.

Table 5
Photocurrent–photovoltage characteristics of the sandwich solar cells. The light intensity is 100 mW cm^{-2}.

No.	Sample	$C_{4\text{-carboxyl pyridine}}$ (mmol L^{-1})	C_{CDCA} (mmol L^{-1})	V_{oc} (V)	J_{sc} (mA cm^{-2})	FF	η/%
1	ZnPc	0.3	0.3	0.35	0.35	0.53	0.065
2	ZnPc	0.3	0	0.32	0.19	0.49	0.030
3	ZnPc	0	0.3	0.34	0.22	0.49	0.037
4	ZnPc	0	0	0.31	0.21	0.40	0.026
5	α-ZnPc(OBu)$_4$	0.3	0.3	0.38	0.65	0.47	0.115
6	α-ZnPc(OBu)$_4$	0.3	0	0.30	0.43	0.52	0.067
7	α-ZnPc(OBu)$_4$	0	0.3	0.32	0.49	0.52	0.081
8	α-ZnPc(OBu)$_4$	0	0	0.28	0.17	0.48	0.023
9	β-ZnPc(OBu)$_4$	0.3	0.3	0.38	0.37	0.53	0.075
10	β-ZnPc(OBu)$_4$	0.3	0	0.32	0.23	0.49	0.036
11	β-ZnPc(OBu)$_4$	0	0.3	0.36	0.32	0.52	0.060
12	β-ZnPc(OBu)$_4$	0	0	0.29	0.22	0.47	0.030

no peak near 1200 cm^{-1} is observed for **ZnPca** proves our identification that the strongest peak at 1201 or 1211 cm^{-1} in the IR spectra of **ZnPcb** or **ZnPcc**, respectively, is mainly due to the C—O unsymmetrical stretching together with some contribution from the phthalocyanine skelecton vibration. For the unsubstituted analogue **ZnPca**, the strongest peak appears at 1336 cm^{-1} contributed by benzene C—C stretching and C—N stretching, which also exists in the spectra of **ZnPcb** and **ZnPcc** but takes a very slightly blue shift due to the *n*-butyoxyl groups. It is noteworthy that the strong peaks observed in the region of 1595–1600 cm^{-1} for **ZnPcb** and **ZnPcc** disappear in **ZnPca**. The new strong peaks are connected with the vibrational modes associated with the oxygen atoms with the assistance of animated pictures produced based on the normal coordinates [37]. Therefore, the electron-donating groups have a relatively large impact on the infrared spectra of phthalocyanine complexes.

3.7. Dye-sensitized solar-cell performances

To further confirm the directional charge transfer in the self-assembled donor–acceptor dyads, the role of 4-carboxyl pyridine coordinated to the zinc atoms of the phthalocyanine macrocycles in the photovoltaic behavior was investigated. In order to reduce the aggregation of dye molecules and improve the cell performance, dye solutions containing 0 or 0.3 mmol L^{-1} chenodeoxycholic acid (CDCA) were used for the sensitization. The dye solutions were prepared in the concentration of 0.3 mmol L^{-1} in toluene/THF (10:1 v:v). The short-circuit currents (J_{sc}), open-circuit potentials (V_{oc}), fill factors (FF), and overall conversion efficiencies (η) of DSSC sensitized under different conditions are summarized in Table 5. While J_{sc} and V_{oc} were registered from experiments using a sandwich solar cell. The overall solar conversion efficiency, η, for a solar cell is given by the photocurrent density measured at short-circuit J_{sc}, open-circuit V_{oc}, the fill factor of the cell (FF), and the intensity of the incident light (P_{in}).

$$\eta = \frac{J_{sc}\, V_{oc}\, FF}{P_{in}} \quad (1)$$

where P_{in} is the total solar power incident on the cell, 100 mW cm^{-2} for air mass (AM) 1.5G.

The fill factor can assume values between 0 and less than 1 and is defined by the ratio of the maximum power (P_{max}) of the solar cell per unit area divided by the J_{sc} and V_{oc} according to

$$FF = \frac{P_{max}}{J_{sc}\, V_{oc}} \quad (2)$$

The maximum power is obtained as the product of the photocurrent and photovoltage at the voltage where the power output of the cell is maximal.

For the ZnPc system, as can be seen from Table 5 and Fig. 6, the DSSC sensitized in the ZnPc solution with the addition of 4-carboxyl pyridine and CDCA possesses the best performance, and it yields a 0.065% efficiency with J_{sc} = 0.35 mA cm^{-2}, V_{oc} = 0.35 V, and FF = 0.53. It can be due to the formation of self-assembled complex **ZnPca**, which causes excited energy transfer from the donor phthalocyanine macrocycle to the acceptor 4-carboxyl pyridine, followed by photoinduced electron transfer to produce charge-separated species [26]. On the other hand, the carboxyl group in the axial direction facilitates the dye molecule to bind to the TiO_2 film electrodes, ensuring efficient electron injection into the TiO_2 conduction band and preventing gradual leaching by the electrolyte. Meanwhile, CDCA effectively suppresses the dye aggregation on the surface of the TiO_2 electrode, and significantly improves the performance of the solar cells [27]. Without the addition of 4-carboxyl pyridine or CDCA, the photovoltaic performance reduces, which can be explained by the unstable physical adsorption of ZnPc as well as no directional charge transfer to the TiO_2 conduction band, or the serious aggregation of **ZnPca** on the TiO_2 electrode [38]. Therefore, in the lack of 4-carboxyl pyridine and CDCA, the photovoltaic performance is the poorest.

For the α-ZnPc(OBu)$_4$ and β-ZnPc(OBu)$_4$ systems, the results show that the variation is similar to the ZnPc system. As shown in Table 5 and Fig. 6, the **ZnPcc**-sensitized solar cell in the presence of CDCA gives a relatively high conversion efficiency of 0.115% with a J_{sc} of 0.65 mA cm^{-2} and V_{oc} of 0.38 V, whereas the **ZnPcb**-sensitized solar cell with CDCA shows an overall efficiency of 0.075% with a J_{sc} of 0.37 mA cm^{-2} and V_{oc} of 0.38 V. As can be seen, as sensitizers in DSSC, **ZnPcc** substituted at α positions performs better than **ZnPcb** substituted at β positions, which can be attributed to the more efficient electronic coupling between phthalocyanine macrocycle and *n*-butyoxyl groups, and the better directional charge transfer. Furthermore, the moving up of the LUMO level of **ZnPcc** increases the driving force for electron injection, which leads to better photovoltaic performance [39–41]. On the other hand, in DSSC the

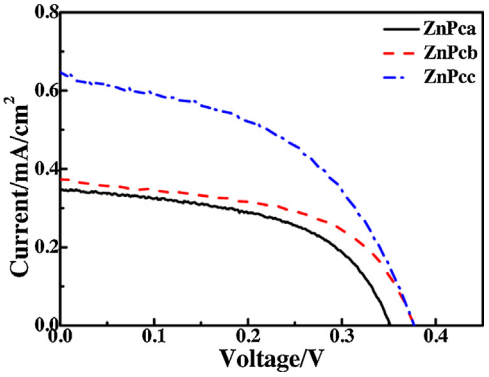

Fig. 6. The best photocurrent–photovoltage characteristics of sandwich solar cells based on **ZnPca**, **ZnPcb** or **ZnPcc**-sensitized-TiO_2 electrode. The light intensity was 100 mW/cm^2.

performances of **ZnPcb** and **ZnPcc** are superior to **ZnPca**, which is mainly due to the introduction of *n*-butyoxyl groups effective preventing the aggregation of dye molecules and reducing the electrons recombination, as well as higher LUMO levels increasing the driving force for electron injection.

4. Conclusions

The molecular structures, atomic charges, molecular orbital energy gaps, molecular orbital spatial distribution, UV–vis spectra and IR spectra of **ZnPca**, **ZnPcb** and **ZnPcc** complexes have been provided by DFT and TDDFT calculations. By comparative study of the self-assembled complexes, it is found that the substitution of the electron-donating *n*-butyoxyl groups at the peripheral positions of phthalocyanine ring adds obvious and different effects to properties of the self-assembled complexes. It is worthwhile to stress that all of the complexes can theoretically provide driving forces for injecting an electron into the TiO_2 surface and for being regenerated by the I_3^-/I^- couple. Additionally, the application of the complexes as sensitizers in DSSC was explored, and the results show that the formation of self-assembled dyads and the addition of the co-adsorbent will decrease the aggregation of the dye molecules, and in turn increase the DSSC performances. The introduction of *n*-butyoxyl groups is effective in tuning both their UV–vis absorption property and molecular orbital energy levels, which induces the improvement of the DSSC performances. In conclusion, the theoretical research agrees very well with the experiment, which proves the directionality of charge transfer in the self-assembled donor–acceptor dyads. Furthermore, this work provides a good method for the application of symmetric phthalocyanines in DSSC.

Acknowledgements

This work was supported by the National Natural Science Foundation of China (21271146, 21271144, 20973128, and 20871096), the Fundamental Research Funds for the Central Universities (2042014kf0228) and the Funds for Creative Research Groups of Hubei Province (2014CFA007), China.

Appendix A. Supplementary data

Supplementary data associated with this article can be found, in the online version, at http://dx.doi.org/10.1016/j.jmgm.2015.04.005

References

[1] D. Gust, T.A. Moore, A.L. Moore, Solar fuels via artificial photosynthesis, Acc. Chem. Res. 42 (2009) 1890–1898.
[2] D. Gust, T.A. Moore, A.L. Moore, Mimicking photosynthetic solar energy transduction, Acc. Chem. Res. 34 (2001) 40–48.
[3] M.R. Wasielewski, Self-assembly strategies for integrating light harvesting and charge separation in artificial photosynthetic systems, Acc. Chem. Res. 42 (2009) 1910–1921.
[4] M.T. Vagnini, A.L. Smeigh, J.D. Blakemore, S.W. Eaton, N.D. Schley, F. D'Souza, R.H. Crabtree, G.W. Brudvig, M.R. Wasielewski, Ultrafast photodriven intramolecular electron transfer from an iridium-based water-oxidation catalyst to perylene diimide derivatives, Proc. Natl. Acad. Sci. U.S.A. 109 (2012) 15651–15656.
[5] G. Bottari, G. de la Torre, D.M. Guldi, T. Torres, Covalent and noncovalent phthalocyanine–carbon nanostructure systems: synthesis, photoinduced electron transfer, and application to molecular photovoltaics, Chem. Rev. 110 (2010) 6768–6816.
[6] T. Hasobe, Supramolecular nanoarchitectures for light energy conversion, Phys. Chem. Chem. Phys. 12 (2010) 44–57.
[7] H. Imahori, T. Umeyama, K. Kurotobi, Y. Takano, Self-assembling porphyrins and phthalocyanines for photoinduced charge separation and charge transport, Chem. Commun. 48 (2012) 4032–4045.
[8] F. D'Souza, O. Ito, Photosensitized electron transfer processes of nanocarbons applicable to solar cells, Chem. Soc. Rev. 41 (2012) 86–96.
[9] J. Deisenhofer, O. Epp, K. Miki, R. Huber, H. Michel, X-ray structure analysis of a membrane protein complex: electron density map at 3 Å resolution and a model of the chromophores of the photosynthetic reaction center from rhodopseudomonas viridis, J. Mol. Biol. 180 (1984) 385–398.
[10] J. Deisenhofer, J.R. Norris, Photosynthetic Reaction Center, Academic Press, San Diego, CA, 1993.
[11] V.M. Blas-Ferrando, J. Ortiz, L. Bouissane, K. Ohkubo, S. Fukuzumi, F. Fernández-Lázaro, Á. Sastre-Santos, Rational design of a phthalocyanine–perylenediimide dyad with a long-lived charge-separated state, Chem. Commun. 48 (2012) 6241–6243.
[12] F.J. Céspedes-Guirao, K. Ohkubo, S. Fukuzumi, A. Sastre-Santos, F. Fernández-Lázaro, Synthesis and photoinduced electron transfer of phthalocyanine–perylenebisimide pentameric arrays, J. Org. Chem. 74 (2009) 5871–5880.
[13] V. Balzani, A. Credi, M. Venturi, Venturi Margherita, Photochemical conversion of solar energy, ChemSusChem 1 (2008) 26–58.
[14] K. Okamoto, S. Fukuzumi, Hydrogen bonds not only provide a structural scaffold to assemble donor and acceptor moieties of zinc porphyrin–quinone dyads but also control the photoinduced electron transfer to afford the long-lived charge-separated states, J. Phys. Chem. B 109 (2005) 7713–7723.
[15] S. Fukuzumi, T. Honda, K. Ohkubo, T. Kojima, Charge separation in metallomacrocycle complexes linked with electron acceptors by axial coordination, Dalton Trans. (20) (2009) 3880–3889.
[16] M.E. El-Khouly, C.A. Wijesinghe, V.N. Nesterov, M.E. Zandler, S. Fukuzumi, F. D'Souza, Ultrafast photoinduced energy and electron transfer in multi-modular donor–acceptor conjugates, Chem. Eur. J. 18 (2012) 13844–13853.
[17] F. D'Souza, E. Maligaspe, K. Ohkubo, M.E. Zandler, N.K. Subbaiyan, S. Fukuzumi, Photosynthetic reaction center mimicry: low reorganization energy driven charge stabilization in self-assembled cofacial zinc phthalocyanine dimer-fullerene conjugate, J. Am. Chem. Soc. 131 (2009) 8787–8797.
[18] S. Fukuzumi, K. Saito, K. Ohkubo, T. Khoury, Y. Kashiwagi, M.A. Absalom, S. Gadde, F. D'Souza, Y. Araki, O. Ito, Multiple photosynthetic reaction centres composed of supramolecular assemblies of zinc porphyrin dendrimers with a fullerene acceptor, Chem. Commun. 47 (2011) 7980–7982.
[19] S. Fukuzumi, K. Saito, K. Ohkubo, V. Troiani, H. Qiu, S. Gadde, F. D'Souza, N. Solladié, Multiple photosynthetic reaction centres using zinc porphyrinic oligopeptide–fulleropyrrolidine supramolecular complexes, Phys. Chem. Chem. Phys. 13 (2011) 17019–17022.
[20] F. D'Souza, P.M. Smith, S. Gadde, A.L. McCarty, M.J. Kullman, M.E. Zandler, M. Itou, Y. Araki, O. Ito, Supramolecular triads formed by axial coordination of fullerene to covalently linked zinc porphyrin–ferrocene(s): design, syntheses, electrochemistry, and photochemistry, J. Phys. Chem. B 108 (2004) 11333–11343.
[21] F. D'Souza, G.R. Deviprasad, M.E. Zandler, V.T. Hoang, A. Klykov, M. VanStipdonk, A. Perera, M.E. El-Khouly, M. Fujitsuka, O. Ito, Spectroscopic, electrochemical, and photochemical studies of self-assembled via axial coordination zinc porphyrin–fulleropyrrolidine dyads, J. Phys. Chem. A 106 (2002) 3243–3252.
[22] K. Harada, M. Fujitsuka, A. Sugimoto, T. Majima, Electron transfer from the S1 and S2 states of pentacoordinated tetrapyrrole macrocycles to pyromellitic diimide as an axial ligand, J. Phys. Chem. A 111 (2007) 11430–11436.
[23] V. Bandi, M.E. El-Khouly, V.N. Nesterov, P.A. Karr, S. Fukuzumi, F. D'Souza, Self-assembled via metal–ligand coordination AzaBODIPY-zinc phthalocyanine and AzaBODIPY-zinc naphthalocyanine conjugates: synthesis, structure, and photoinduced electron transfer, J. Phys. Chem. C 117 (2013) 5638–5649.
[24] Y.-O. Yeung, R.C. Liu, W.-F. Law, P.-L. Lau, J. Jiang, D.K. Ng, Synthetic studies of substituted 2,3-naphthalocyanines, Tetrahedron 53 (1997) 9087–9096.
[25] D.K. Ng, Y.-O. Yeung, W.K. Chan, S.-C. Yu, Columnar liquid crystals based on 2,3-naphthalocyanine core, Tetrahedron Lett. 38 (1997) 6701–6704.
[26] L.J. Yu, W.Y. Shi, L. Lin, Y.W. Liu, R.J. Li, T.Y. Peng, X.G. Li, Effects of benzoannelation of asymmetric phthalocyanine on the photovoltaic performance of dye-sensitized solar cells, Dalton Trans. 43 (2014) 8421–8430.
[27] L.J. Yu, K. Fan, T.N. Duan, X.G. Chen, R.J. Li, T.Y. Peng, Efficient panchromatic light harvesting with co-sensitization of zinc phthalocyanine and bithiophene-based organic dye for dye-sensitized solar cells, ACS Sustainable Chem. Eng. 2 (2014) 718–725.
[28] A.D. Becke, Density-functional thermochemistry III. The role of exact exchange, J. Chem. Phys. 98 (1993) 5648–5652.
[29] P.J. Hay, W.R. Wadt, Ab initio effective core potentials for molecular calculations, potentials for the transition metal atoms Sc to Hg, J. Chem. Phys. 82 (1985) 270–283.
[30] W.R. Wadt, P.J. Hay, Ab initio effective core potentials for molecular calculations. Potentials for main group elements Na to Bi, J. Chem. Phys. 82 (1985) 284–298.
[31] (a) P.J. Hay, W.R. Wadt, Ab initio effective core potentials for molecular calculations. Potentials for K to Au including the outermost core orbitals, J. Chem. Phys. 82 (1985) 299–310;
(b) L. Wan, D. Qi, Y. Zhang, J. Jiang, Controlling the directionality of charge transfer in phthalocyaninato zinc sensitizer for a dye-sensitized solar cell: density functional theory studies, Phys. Chem. Chem. Phys. 13 (2011) 1639–1648.
[32] (a) X. Cai, Y.X. Zhang, X.X. Zhang, J.Z. Jiang, Structures and properties of 2,3,9,10,16,17,23,24-octasubstituted phthalocyaninato-lead complexes: the substitutional effect study on the basis of density functional theory calculations, J. Mol. Struct.—THEOCHEM 801 (2006) 71–80;
(b) A. Zhong, Y. Zhang, Y. Bian, Structures and spectroscopic properties of nonperipherally and peripherally substituted metal-free phthalocyanines: a substitution effect study based on density functional theory calculations, J. Mol. Graph. Modell. 29 (2010) 470–480.

[33] L.L. Yang, L.H. Guo, Q.Q. Chen, H.F. Sun, J. Liu, X.X. Zhang, X. Pan, S.Y. Dai, Theoretical design and screening of panchromatic phthalocyanine sensitizers derived from TT1 for dye-sensitized solar cells, J. Mol. Graph. Modell. 34 (2012) 1–9.
[34] (a) M.E. Ragoussi, J.J. Cid, J.H. Yum, G. de la Torre, D. Di Censo, M. Gratzel, M.K. Nazeeruddin, T. Torres, Carboxyethynyl anchoring ligands: a means to improving the efficiency of phthalocyanine-sensitized solar cells, Angew. Chem. Int. Ed. 51 (2012) 4375–4378;
(b) R. Ma, P. Guo, H. Cui, X. Zhang, M.K. Nazeeruddin, M. Grätzel, Substituent effect on the meso-substituted porphyrins: theoretical screening of sensitizer candidates for dye-sensitized solar cells, J. Phys. Chem. A 113 (2009) 10119–10124.
[35] S.B. Ko, A.N. Cho, M.J. Kim, C.R. Lee, N.G. Park, Alkyloxy substituted organic dyes for high voltage dye-sensitized solar cell: effect of alkyloxy chain length on open-circuit voltage, Dyes Pigm. 94 (2012) 88–98.
[36] X. Zhang, Y. Zhang, J. Jiang, Towards clarifying the N–M vibrational nature of metallo-phthalocyanines infrared spectrum of phthalocyanine magnesium complex: density functional calculations, Spectrochim. Acta, A: Mol. Biomol. Spectrosc. 60 (2004) 2195–2200.
[37] X.D. Gong, H.M. Xiao, H. Tian, Comparative studies on the structures, infrared spectrum, and thermodynamic properties of phthalocyanine using ab initio Hartree–Fock and density functional theory methods, Int. J. Quantum. Chem. 86 (2002) 531–540.
[38] M. Kimura, H. Nomoto, H. Suzuki, T. Ikeuchi, H. Matsuzaki, T.N. Murakami, A. Furube, N. Masaki, M.J. Griffith, S. Mori, Molecular design rule of phthalocyanine dyes for highly efficient near-IR performance in dye-sensitized solar cells, Chem. Eur. J. 19 (2013) 7496–7502.
[39] N. Kobayashi, H. Ogata, N. Nonaka, E.A. Luk'yanets, Effect of peripheral substitution on the electronic absorption and fluorescence spectra of metal-free and zinc phthalocyanines, Chem. Eur. J. 9 (2003) 5123–5134.
[40] N. Kobayashi, N. Sasaki, Y. Higashi, T. Osa, Regiospecific and nonlinear substituent effects on the electronic and fluorescence spectra of phthalocyanines, Inorg. Chem. 34 (1995) 1636–1637.
[41] M.K. Nazeeruddin, R. Splivallo, P. Liska, P. Comte, M. Grätzel, A swift dye uptake procedure for dye sensitized solar cells, Chem. Commun. (12) (2003) 1456–1457.